Chemical Geology 476 (2018) 340–351

Contents lists available at ScienceDirect

Chemical Geology

journal homepage: www.elsevier.com/locate/chemgeo

Variations and controls of iron oxides and isotope compositions during paddy soil evolution over a millennial time scale

Lai-Ming Huang[a,b,c,d,*], Xiao-Xu Jia[a,c,d], Gan-Lin Zhang[b,c,**], Aaron Thompson[e], Fang Huang[f], Min-An Shao[a,c,d], Liu-Mei Chen[g]

[a] Key Laboratory of Ecosystem Network Observation and Modeling, Institute of Geographic Sciences and Natural Resources Research, Chinese Academy of Sciences, Beijing 100101, China
[b] State Key Laboratory of Soil and Sustainable Agriculture, Institute of Soil Science, Chinese Academy of Sciences, Nanjing 210008, China
[c] College of Resources and Environment, University of Chinese Academy of Sciences, Beijing 100049, China
[d] State Key Laboratory of Soil Erosion and Dryland Farming on the Loess Plateau, Institute of Soil and Water Conservation, College of Natural Resources and Environment, Northwest A&F University, China
[e] Department of Crop and Soil Science, University of Georgia, Athens, GA 30602, USA
[f] School of Earth and Space Sciences, University of Science and Technology of China, China
[g] College of Resources and Environment, Zunyi Normal College, Zunyi 563002, China

ARTICLE INFO

Editor: G. Jerome

Keywords:
Fe oxides
Fe isotopes
Paddy soil chronosequence
Anthropedogenesis
Earth's Critical Zone

ABSTRACT

A paddy soil chronosequence consisting of five profiles derived from calcareous marine sediments with cultivation history from 0 to 1000 years was studied to understand the underlying mechanisms and processes controlling the millennial scale Fe evolution. We evaluated the chronosequencial changes in depth distribution of Fe oxide contents and Fe isotopic compositions. Results showed that paddy soil evolution under the influence of periodic flooding and groundwater fluctuation resulted with time in variations of soil moisture regime and redox condition that control Fe mobilization, translocation and redistribution, leading to enhanced profile differentiation of Fe oxides and measurable Fe isotope fractionation. Total Fe and oxide bound Fe as well as their differentiation between surface and subsurface horizons increased as paddy soils age, leading to the formation of diagnostic horizons and features characterizing Fe distribution and redistribution. Selective extractions showed that the weakly-bound, oxide-bound and silicate bound Fe corresponded to 1–16%, 8–46%, and 52–91% of the total Fe, respectively, and these proportions varied with both time and depth due to the redox-related Fe transformation and translocation. δ^{56}Fe values in the studied paddy soil chronosequence ranged from − 0.01‰ to 0.18‰ and exhibited a strong negative correlation with the logarithm of total Fe concentrations, suggesting mass-dependent Fe isotope fractionation occurred as a result of the preferential removal of lighter Fe isotopes during long-term paddy soil evolution under the predominant reducing conditions. However, the Fe isotopic ratio of a specific paddy soil horizon was a result of a complex interaction of different processes, which were summarized and interpreted in our proposed conceptual model. Comparison of Fe isotopic compositions in the worldwide soils demonstrated that Fe isotopes can evidence Fe transfer and pinpoint the factors and processes that control Fe mobilization and redistribution particularly in soils with changing moisture regimes and redox conditions. Our findings provide new insights into the behavior and geochemical cycle of Fe at the Earth's surface strongly affected by human activities and contributes to an improved understanding of how anthropedogenesis affects Fe evolution in the Earth's Critical Zone.

1. Introduction

Iron (Fe) is the fourth most abundant element in the Earth's crust (6.7 wt%) (Rudnick and Gao, 2004), serving as an essential nutrient for almost all living organisms (Bernuzzi and Recalcati, 2006). Its dynamic changes in valence state in response to shifting redox conditions trigger many processes in terrestrial ecosystems, such as mineral weathering, nutrient cycling, and contaminant mobility (Cornell and Schwertmann,

* Correspondence to: L.-M. Huang, Key Laboratory of Ecosystem Network Observation and Modeling, Institute of Geographic Sciences and Natural Resources Research, Chinese Academy of Sciences, Beijing 100101, China.
** Correspondence to: G.-L. Zhang, State Key Laboratory of Soil and Sustainable Agriculture, Institute of Soil Science, Chinese Academy of Sciences, NO. 71 East Beijing Road, Nanjing 210008, China.
E-mail addresses: huanglm@igsnrr.ac.cn (L.-M. Huang), glzhang@issas.ac.cn (G.-L. Zhang).

https://doi.org/10.1016/j.chemgeo.2017.11.030
Received 17 January 2017; Received in revised form 11 August 2017; Accepted 23 November 2017
Available online 26 November 2017

2003). Fe also plays an important role in the preservation of organic carbon in both soils and sediments (Kaiser and Guggenberger, 2000; Lalonde et al., 2012), which contributes to the global carbon cycle and affects climate change (Jickells et al., 2005).

In soils, Fe occurs in a variety of different phases, such as primary silicate minerals, pedogenic clay minerals, Fe (oxyhydr)oxides with different degrees of crystallinity, as well as in organic complexes (Stucki et al., 1988). The weathering of primary silicate minerals in soils releases Fe^{II}, which is rapidly oxidized in oxic environments and precipitated as poorly crystalline Fe (oxyhydr)oxides such as ferrihydrite or lepidocrocite. The Ostwald ripening of these short-range-ordered (SRO) Fe phases to crystalline Fe (oxyhydr)oxides, such as goethite and hematite, takes place during further soil development. Under oxic conditions in well-drained soils, Fe^{III} is the thermodynamic stable oxidation state and characterized by a very low solubility (Cornell and Schwertmann, 2003). Under anoxic conditions in water-saturated soils, however, Fe^{III} provides a terminal electron acceptor for anaerobic respiration of dissimilatory Fe-reducing microorganisms (Lovley et al., 2004), resulting in the formation of the highly soluble Fe^{II} aquoion. In addition to reductive dissolution, mobilization of Fe also occurs via proton-promoted dissolution at pH < pznpc (point of zero net proton charge) and to a greater extent via ligand-promoted dissolution when strong binding organic acids are present (Jansen et al., 2003). The mobile Fe^{II} can be transported within soils by both lateral and vertical diffusion and it is rapidly oxidized and re-precipitated as Fe^{III} in the presence of O_2. The re-precipitation process happens depending on the temporal and spatial variability of soil moisture regimes, resulting in the formation of relatively “Fe-depleted” and “Fe-enriched” micro-sites with distinct redoximorphic features. Thus, the Fe mobilization, translocation, and redistribution as well as the associated Fe mineral transformation are key processes in soil formation influencing the morphological and physico-chemical properties of soils (van Breemen and Buurman, 2004). Understanding the mechanisms and processes that control the behavior and dynamics of Fe in soils is among the fundamental questions in pedology and geochemistry, and will be conducive to assess the function and ecosystem service of Critical Zone responding to the ever-increasing natural and anthropogenic changes.

Previous studies have shown that the natural soil formation involves significant changes in species, amounts, and stability of Fe (oxyhydr) oxides (e.g., Torrent et al., 1980; McFadden and Hendricks, 1985; Diaz and Torrent, 1989; Aniku and Singer, 1990; Cornell and Schwertmann, 2003; Vodyanitskii, 2010) and measureable Fe isotope fractionations (e.g., Fantle and DePaolo, 2004; Emmanuel et al., 2005; Thompson et al., 2007; Wiederhold et al., 2007a, 2007b; Yamaguchi et al., 2007; Buss et al., 2010; Kiczka et al., 2011; Yesavage et al., 2012; Mansfeldt et al., 2012; Fekiacova et al., 2013; Akerman et al., 2014; Schuth et al., 2015; Garnier et al., 2017; Li et al., 2017). The ratio of dithionite-citrate-bicarbonate extractable Fe to total Fe generally increases while the ratio of oxalate extractable Fe to total Fe decreases with increasing pedogenic age as indicated by the selective chemical extractions (Torrent et al., 1980; McFadden and Hendricks, 1985; Diaz and Torrent, 1989; Aniku and Singer, 1990). In addition, the crystallinity of Fe (oxyhydr)oxides and the amount of Al that substitutes Fe in goethite often increase with increasing soil development (Cornell and Schwertmann, 2003; Vodyanitskii, 2010). These changes are caused by weathering of silicate minerals, redox reactions, and the lattice replacement of other metals with Fe in Fe-bearing minerals. Recent analytical advances in MC-ICP-MS (multiple collector inductively plasma mass spectrometry) technology have shown significant deviations of δ^{56}Fe values in soils from that of igneous rocks (e.g., Fantle and DePaolo, 2004; Thompson et al., 2007; Wiederhold et al., 2007a; Fekiacova et al., 2013; Akerman et al., 2014; Schuth et al., 2015; Garnier et al., 2017). The fractionation of Fe isotope in soils can be mediated by abiotic processes (e.g., proton-promoted or ligand-controlled Fe dissolution and mobilization, Fe adsorption and precipitation, as well as mineral transformation), biotic processes (microbial reduction or oxidation of Fe), and a combination of both pathways, which favor the preferential release of light isotope (^{54}Fe) to solution leaving an isotopically heavy solid (enriched in ^{56}Fe) (Johnson et al., 2002, 2008). Contrasting to the well-documented Fe dynamics during natural pedogenesis, a comprehensive understanding of the variations and controls of Fe oxides and Fe isotope compositions during anthropedogenesis of paddy soils strongly affected by human activities is poorly constrained. The natural pedogenic controls on Fe evolution may be superseded by human activities (Dudal, 2005) that alter the rate and trajectory of net Fe dynamics either directly (e.g., Fe additions by irrigation) or indirectly (e.g., Fe transformations by artificial flooding and draining). The combined use of different approaches, such as selective extraction and Fe isotope analysis, for characterizing Fe dynamics would provide a more comprehensive understanding of the mechanisms and processes that control Fe biogeochemical cycling.

Paddy soils make up the largest anthropogenic wetlands on earth and play critical roles in ecosystem functions (Huang et al., 2015). They may originate from many types of soils in pedological terms or different parent materials, but are highly modified by anthropogenic management during paddy cultivation. The periodic artificial flooding and draining as well as groundwater fluctuations during paddy soil evolution result in significant changes in soil moisture regime and redox conditions with both time and depth, which come to govern Fe mobilization, translocation and redistribution (Gong, 1983, 1986; Zhang and Gong, 1993, 2003; Huang et al., 2015). Given the widespread cultivation of rice, paddy soils represent a key component of the Fe geochemical cycle at the Earth's surface. Previous studies have extensively investigated the changing status of Fe oxides (Yu, 1985; Gong, 1986) and Fe isotopes (Garnier et al., 2017) at a given stage of paddy soil evolution through a comparison with the initial parent material. However, little is known about the successive changes of Fe oxides and Fe isotopic composition during paddy soil evolution that is required to identify process rates and thresholds of Fe dynamics.

Paddy soil chronosequence provides a valuable tool for investigating the rates and directions of property changes and the associated environmental thresholds (Huang et al., 2015). In this study, we measured different forms of Fe oxides and the stable Fe isotope compositions in a paddy soil chronosequence consisting of five profiles derived from calcareous marine sediments with cultivation history ranging from 0 to 1000 years (Chen et al., 2011; Huang et al., 2013) (Fig. 1). Our objectives were to (i) investigate the dynamic changes in Fe oxides and Fe isotope compositions during anthropedogenesis of paddy soil; (ii) identify the underlying mechanisms and processes controlling millennial scale Fe evolution; (iii) establish a conceptual model characterizing Fe transfer and redistribution in paddy soils and assess their impacts on Fe isotope fractionation; and (iv) compare Fe isotopic compositions in the worldwide soils and evaluate the potential of using Fe isotopes to record information about Fe transfer and soil formation.

2. Materials and methods

2.1. Study area and sampling sites

The study area is located on a coastal plain in Cixi County, Zhejiang Province, facing the East China Sea, between 121°2′–121°36′ E and 30°2′–30°19′ N (Fig. 1). This region belongs to the southern fringe of northern subtropics and has a mean annual air temperature of 16 °C, with yearly extremes ranging from − 5 °C to 37 °C, and a mean annual precipitation of 1325 mm of which 73% is concentrated in the rice paddy flooding season (i.e., April to October). The coastal plain ranges from 2.6 m to 5.7 m above sea level, and slopes gently towards the northeast (Fig. 1). Soils in the studied area have developed on the marine sediments from the East China Sea, which receives large amounts of terrigenous materials from the nearby Qiantang and Yangtze Rivers (Chen et al., 2011). Step-by-step land reclamation of the

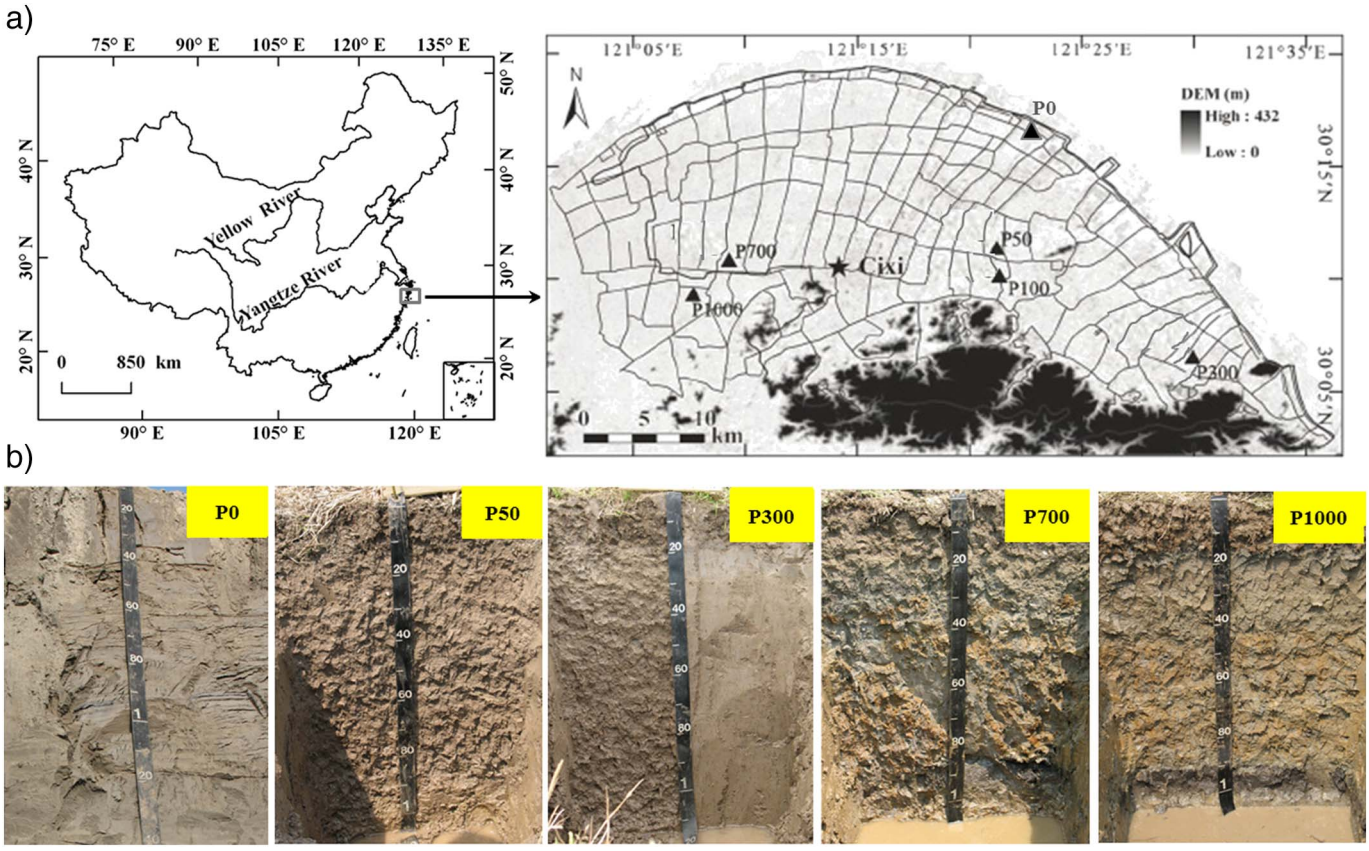

Fig. 1. Location of the study area and sampling sites in Cixi County, Zhejiang Province in Southeast China (a); and representative soil profiles (P0, P50, P300, P700, and P1000) with 0, 50, 300, 700 and 1000 years of rice cultivation history based on the chronology of dyke construction (Wang, 2004) (b).

tidal mudflat through successive dyke building (Wang, 2004) has resulted in a chronosequence with different stages of soil development (Chen et al., 2011). Rice (*Oryza sativa* L.) cultivation in the lower areas where fresh water is readily available for irrigation generally begins after five years of dyke building when the salt concentration decreases to agronomically tolerable levels. Sites with 50, 300, 700 and 1000 years of rice cultivation history (i.e., P50, P300, P700 and P1000) were identified (Fig. 1) based on the chronology of dyke construction (Wang, 2004). In addition, an uncultivated mud beach profile (P0) was selected to represent the original soil (parent material, time zero) of the paddy soils (Fig. 1). The parent material homogeneity in the inter- and intra-profiles of the studied chronosequence (P0, P50, P300, P700, P1000) has been evaluated by making use of various soil attribute parameters (Chen and Zhang, 2009; Chen et al., 2014a). Details of these profiles (P0, P50, P300, P700, and P1000) and the soil chronosequence recognition have been given by Chen et al. (2011, 2014a, 2015) and Huang et al. (2013, 2014).

2.2. Soil sampling and description

Within each area of identical paddy cultivation history, one representative profile was chosen for soil sampling based on soil landscape and geomorphological characteristics of that area. All soil samples were collected when the fields were drained after rice harvest. Soil profiles were described and sampled according to genetic horizons following standard field description guidelines (Schoeneberger et al., 2002; FAO, 2006). The uncultivated soil profile was generally homogeneous throughout its depth, with no observable horizon differentiation (Fig. 1b, and Table S1 in Supplementary File S1). In contrast, the paddy soil profiles showed complicated patterns with depth due to anthropedogenesis and consisted of an anthrostagnic epipedon, including the cultivated horizon (Ap1) and the plow pan (Ap2), and a hydragric horizon (Bg) (Fig. 1b, and Table S1 in Supplementary File S1). Differences in morphological properties, including soil color, texture and redoximorphic features, were also evident between the relatively younger pedons (50–300 years) and the older ones (700–1000 years) (Fig. 1b, and Table S1 in Supplementary File S1). Soils were defined as Primosol (P0), Hapi-Stagnic Anthrosol (P50 and P300), Fe-leachi-Stagnic Anthrosol (P700), and Fe-accumuli-Stagnic Anthrosol by referring to Chinese Soil Taxonomy (Cooperative Research Group on Chinese Soil Taxonomy, 2001) (Table S1 in Supplementary File S1). The detailed field descriptions and classifications of the soil profiles are given in Table S1 in Supplementary File S1.

2.3. Analysis of basic soil physicochemical properties

After collection, samples of each soil horizon were dried at room temperature and then gently crushed using a wooden pestle and mortar and passed through a 2-mm nylon sieve. Soil bulk density was measured on the 100 cm^{-3} undisturbed soil cores by drying the cores for 24 h at 105 °C. The particle size distribution was determined by the pipette method and the clay content was defined as the mass percentage of particles < 2 μm in diameter for the whole soil. Soil pH was determined at a 1:2.5 soil/solution ratio using distilled water and the carbonate content was determined using a Dietrich Fruhling pressure calcimeter according to the Institute of Soil Science, Chinese Academy of Sciences (1978). Soil organic carbon (SOC) was measured by the Walkley-Black wet oxidation method (Nelson and Sommers, 1982) using the 149-μm fraction. Total nitrogen (N_{tot}) was measured by Kjeldahl method (Bremner, 1960) and total phosphorus (P_{tot}) was determined by $HClO_4$-HF digestion followed by colorimetric analysis (Institute of Soil Science, Chinese Academy of Sciences, 1978). For total elemental analysis, soil samples (< 74 μm) were fused by a mixture of 1:1 lithium metaborate and lithium tetraborate for 30 min in a 1000 °C

muffle furnace and then were dissolved in 10% HNO_3 + 1% HF solution. Total elemental concentrations including K, Na, Ca, Mg, Fe, Mn, Al, Si, Ti, and Zr were determined by inductively coupled plasma-optical emission spectrometry. We estimate the precision as 5–10% relative standard deviation based on replicates and standard samples (Geochemical Standard Reference Sample Soil, GSS-3). The measured data are listed in Table S2 in Supplementary File S1. Briefly, the studied chronosequence on a millennium time scale showed three phases of paddy soil evolution: an initial phase during the first few decades (0–50 years) dominated by rapid desalinization, accumulation of topsoil organic matter and formation of a compacted plow pan (Tables S1 and S2 in Supplementary File S1); the second phase lasts several centuries (50–700 years) comprising Fe and clay enrichment in the illuvial horizon, and the loss of phosphorus and Mn coincident with the near complete removal of $CaCO_3$ (Table S2 in Supplementary File S1); in the third phase (> 700 years), (trans-)formation and redistribution of metal oxides are accompanied by clearly visible hydromorphic patterns in paddy subsoils (Table S1 in Supplementary File S1, and Fig. 1b). The details of dynamic changes in basic soil physicochemical properties have been given by Chen et al. (2011), who investigated pedogenic response times and thresholds.

2.4. Extraction of Fe oxides and measurement of Fe concentrations

Bulk soil samples were subjected to reducing agents with increasing strength to selectively extract major pools of Fe: (1) the Tamm's extraction (Tamm, 1922); and (2) the citrate-bicarbonate-dithionite (CBD) extraction (Mehra and Jackson, 1960). The Tamm's extraction is a mixture of oxalic acid and ammonium oxalate, which was performed by shaking the sample-solution mixture in the dark over 4 h at 20 °C with a solid/liquid ratio of 1.25 g/50 ml. The Tamm's method targets the extraction of weakly bound, short-range-ordered (SRO) and organic bound Fe (Duchaufour and Souchier, 1966). For the extraction by CBD, soil samples were exposed to the reactant mixture at 80 °C for 30 min with a solid/liquid ratio of 0.5 g/25 ml. The CBD method extracts Fe in oxides and hydroxides (e.g., hematite, goethite, lepidocrocite) of all crystallinities—SRO and bulk crystalline (Mehra and Jackson, 1960). In addition to the partial extractions, total Fe was dissolved in a HF-$HClO_4$ mixture after calcination of soil organic matter at 450 °C. Fe concentrations in the extracted solutions were analyzed using an Inductively Coupled Plasma-Atomic Emission Spectrometer (ICP-AES, LAS Arras). We calculated the oxide bound Fe concentration by subtracting oxalate-extractable Fe from the CBD-extractable Fe and the silicate bound Fe was calculated by subtracting CBD-extractable Fe from the total Fe concentration.

2.5. Fe purification and Fe isotope measurements

An aliquot of powdered sample (< 74 μm, 100–500 mg depending on Fe content) was treated with 30% H_2O_2 to destroy organic matter and then was dissolved completely in a microwave digestion with HF-HNO_3-HCl (1:1:3) for 30 min at 150 °C. Samples with high organic matter were digested for 1 h in order to obtain a complete digestion, despite that organic matter was removed before digestion. In addition, the digested clear solutions were evaporated in Teflon beakers on a hotplate and oxidized with HNO_3 and H_2O_2 to remove the potential remaining organic compounds and hydroxylamine and to convert Fe^{2+} to Fe^{3+}. The residue of this evaporation was re-dissolved in 6 M HCl for Fe separation and purification. Solution aliquots containing 100 μg Fe were purified using 1 ml of pre-cleaned anion exchange resin (Bio-Rad AG1 X4, 200–400 mesh) in 10 ml Bio-Rad polypropylene column (Bio-Rad #731-1550) in a metal-free clean chemistry laboratory following the procedure outlined in Wiederhold et al. (2007a, 2007b). Prior to purification, the anion exchange resin was cleaned according to Thompson et al. (2007). During the double chromatographic separation processes, Fe^{3+} was present as the $FeCl_4^-$ anion in 6 M HCl. The Fe complex was retained on the resin while the sample matrix was washed out by the repeated additions of 6 M HCl. Quantitative elution of Fe from the columns was achieved with 0.05 M HCl. The final eluted sample was evaporated to dryness with 1 drop of 30% H_2O_2 to ensure that all the Fe was in ferric form and then was re-dissolved in 0.3 M HNO_3. All the acids used during purification were cleaned in Teflon distills at sub-boiling conditions and prepared with ultrapure water (> 18 MX cm, Milli-Q, Millipore, USA). Recovery of Fe from the column after purification was found to be > 98% and the analytical blank was negligible (< 10 ng Fe) relative to the amounts of Fe (100 μg) loaded onto the columns.

Fe isotopic measurements were carried out at USTC (University of Science and Technology of China, Hefei) using a high-resolution multiple collector inductively coupled plasma mass spectrometer (MC-ICP-MS, Neptune Plus, Thermo Fisher Scientific) following the analytical procedure described by Schuth et al. (2015). Comprehensive descriptions of Fe isotope analytical methods were published by Schoenberg and von Blanckenburg (2005) and de Jong et al. (2007). Briefly, a standard-bracketing approach with IRMM-014 as standard reference material was used to correct for machine drift and instrumental mass bias (i.e., standard-sample-standard bracketing). The sample solution was introduced into the plasma via a quartz glass double pass spray chamber combined with a PFA nebulizer. Interferences of $^{40}Ar^{14}N^+$, $^{40}Ar^{16}O^+$, and $^{40}Ar^{16}OH^+$ on the peaks of $^{54}Fe^+$, $^{56}Fe^+$ and $^{57}Fe^+$ were sufficiently resolved in medium resolution mode, thereby providing interference-free signal plateaus for Fe isotope measurements. Fe isotopic compositions were reported using standard delta notation in units of per mil (‰) relative to the international Fe isotope standard IRMM-014 using the following equation:

$$\delta^{56}Fe(‰) = \left[\frac{(^{56}Fe/^{54}Fe)sample}{^{56}Fe/^{54}Fe_{IRMM\text{-}014}} - 1\right] \times 10^3 \quad (1)$$

Each sample and standard was measured at least four times and there was a replicate every ten samples. Mass spectrometric reproducibility was tested by running the IRMM-014 standard both as sample and as standard. Procedural errors were determined by processing IRMM-014 solution samples using the same double chromatographic separation protocol as the soil samples. The precision of the isotopic compositions calculated on the basis of repeated measurements of the IRMM-014 standard was 0.04‰ (2SD) and 0.05‰ (2SD) for $\delta^{56}Fe$ and $\delta^{57}Fe$, respectively. The 2SD of $\delta^{56}Fe$ values of the soil samples with repeated measurements were < 0.06‰ (Table S3 in Supplementary File S1). In a $\delta^{57}Fe$ vs. $\delta^{57}Fe$ diagram, all soil sample and standard measurements plotted along a line with a slope of 1.471 (Fig. S1). This value is equal, within error margins, to the theoretical value of ln(M57/M6) / ln(M56/M54) = 1.487, indicating mass-dependent fraction and no influence of isobaric interferences.

2.6. Data analyses and calculations

Fe mass (kg m^{-2}) in the soil pedon was calculated by multiplying Fe concentrations by bulk density and thickness of soil horizons using the following equation:

$$Fe_{mass} = \sum_i^n C_{Fe} D_i E_i / 100 \quad (2)$$

where C_{Fe}, D_i, and E_i is, respectively, the Fe concentration (g kg^{-1}), bulk density (g cm^{-3}) and depth (cm) in the *i* horizon.

Loss and gain of Fe was computed by applying a simplified version of the open-system transport function (Brimhall and Dietrich, 1987; Chadwick et al., 1990), which ignored physical collapse and dilation of the soil column. The mass fraction of Fe lost or gained from a soil horizon relative to the mass of Fe originally present in the parent material was calculated using the following expression:

$$\tau_{Ti,Fe} = \frac{C_{Fe,w} C_{Ti,p}}{C_{Fe,p} C_{Ti,w}} - 7 \quad (3)$$

Here, C refers to the concentration (mg kg^{-1}) of immobile (Ti) and mobile (Fe) elements in the weathered (w) or parent (p) material. For the studied paddy soil chronosequence, Ti has been determined to be the least mobile element (Chen et al., 2014a). Values of $\tau_{Ti,Fe} > 0$ indicate that Fe is enriched in soil relative to parent material, while $\tau_{Ti,Fe} < 0$ indicates depletion and the absolute value of $\tau_{Ti,Fe}$ reveals the fraction of Fe left in soil relative to the parent material for the depleted samples.

Relationships between Fe concentrations and Fe isotopic ratios were analyzed by linear regression analysis, including regression diagnostics to ensure model appropriateness. Simple Pearson correlation coefficients among different soil properties were calculated. All statistical analyses were performed in the Statistical Package for the Social Sciences program (SPSS 13.0 for Windows, Chicago, IL, USA).

3. Results

3.1. Fe concentrations

Total Fe concentration and distribution was uniform throughout the soil profile in the uncultivated pedon (P0), ranging from 28.22 to 30.34 g kg^{-1} (Fig. 2, and Table S3 in Supplementary File S1). A measurable profile differentiation of total Fe was observed in all of the paddy soils (Fig. 2), suggesting a transport and redistribution of Fe during paddy soil evolution. The standard deviation of total Fe concentration within 120 cm profile increased rapidly from 0.92 in the uncultivated pedon (P0) to 12.44 in the oldest paddy soil (P1000). This variation occurred as total Fe accumulated in the illuvial horizons (Bg or Btg) while it remained relatively constant in the surface and subsurface horizons (Ap1 and Ap2) during paddy soil evolution (Fig. 2, and Table S3 in Supplementary File S1). In addition, there was a measurable decline of total Fe concentration in the horizons near groundwater table (e.g., 110 cm in P300, 100 cm in P700, and 90 cm in P1000) as compared with that in the illuvial horizons in the older paddy soils (Fig. 2). The weighted-mean total Fe concentration within 120 cm profile increased gradually in the studied paddy soil chronosequence (P0, 29.50 g kg^{-1}; P50, 36.55 g kg^{-1}; P300, 37.69 g kg^{-1}; P700, 39.72 g kg^{-1}; P1000, 42.51 g kg^{-1}), suggesting an accumulation of total Fe as paddy soils age. This was further confirmed by the positive values of $\tau_{Ti,Fe}$ in most horizons of the paddy soil profiles (Table S3 in Supplementary File S1).

Selective extractions showed that the contributions of different Fe pools to total Fe varied along the soil depth and chronosequence (Fig. 2, and Table S3 in Supplementary File S1). The oxide bound Fe corresponded to 8–46% of the total Fe in the studied paddy soil chronosequence (Table S3 in Supplementary File S1) and its vertical distribution and evolution mimicked that of total Fe (Fig. 2). This resulted in a strong correlation between the oxide bound Fe and total Fe, with a correlation coefficient of 0.94 ($n = 30$, $p < 0.01$) (Fig. S2 in Supplementary File S1). The weakly bound, poorly crystalline Fe pool corresponded to 1–16% of the total Fe (Table S3 in Supplementary File S1) and was present at consistently lower concentrations than in the parent material (Fig. 2). The silicate bound Fe represented 52–91% of the total Fe (Table S3 in Supplementary File S1) and its concentration tended to increase with soil depth and increasing paddy cultivation age (Fig. 2).

3.2. Fe isotopic compositions

The δ^{56}Fe and its distribution was uniform (ranging from 0.05‰ to 0.07‰) throughout the soil profile in the uncultivated pedon (P0), corresponding to the relatively constant Fe concentrations (Fig. 3, and Table S3 in Supplementary File S1). This indicated virtually no vertical fractionation of Fe isotopes in the young Cambisol (i.e., the uncultivated pedon P0). In contrast, the amplitude of the Fe isotopic variations was much larger than the external reproducibility within the cultivated paddy soil profiles. The Fe isotopic compositions (δ^{56}Fe) of the studied paddy soil chronosequence varied from −0.01‰ to 0.18‰ (Fig. 3, and Table S3 in Supplementary File S1) corresponding to the large fluctuations of Fe concentrations during paddy soil evolution (Fig. 3, and Table S3 in Supplementary File S1). This suggests Fe isotope fractionation occurs during the millennial scale paddy soil evolution.

The δ^{56}Fe values in the surface and subsurface horizons of paddy soils (0.07‰–0.17‰) were higher than that of the parent material (0.05‰–0.07‰) and tended to increase with the prolonged rice cultivation age (Fig. 3, and Table S3 in Supplementary File S1). However, the lowest δ^{56}Fe value in each paddy soil profile was observed in the illuvial horizons (Bg or Btg) and decreased as paddy soils age, inversely correlated with an increase in total Fe concentration (Fig. 3, and Table S3 in Supplementary File S1). Relative to the illuvial horizons, the deeper horizons near the groundwater level decreased in total Fe concentration while their δ^{56}Fe values increased as the paddy soils age (Fig. 3, and Table S3 in Supplementary File S1). The horizons below groundwater level in the 700-yr and 1000-yr paddy soil exhibited lower δ^{56}Fe values than the horizons immediate above. The Ab horizons of 700-yr (P700, 90–112 cm) and 1000-yr (P1000, 85–100 cm) paddy profile, which were buried A horizons rich in humus and depleted in Fe, showed much higher δ^{56}Fe values than those in the illuvial horizons (Fig. 3, Tables S2 and S3 in Supplementary File S1).

4. Discussions

4.1. Fe redistribution and accumulation during paddy soil evolution

Fe is mobilized and translocated within profile during paddy soil evolution as evidenced by the increasing differentiation of Fe mass and speciation within different selective extractions across the paddy soil chronosequence (Fig. 2). Our results are consistent with prior observations that rice cultivation influences Fe differentiation within paddy soils, irrespective of parent material (Gong, 1983, 1986; Yu,

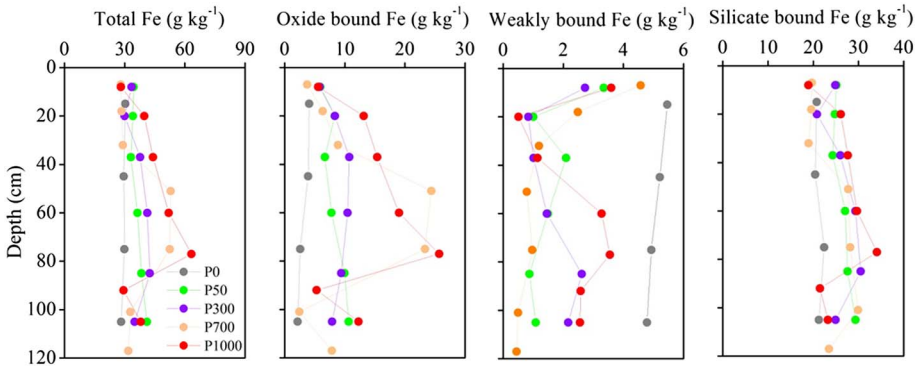

Fig. 2. Distributions and variations of total Fe, oxide bound Fe, weakly bound Fe, and silicate bound Fe concentrations along the soil depth and chronosequence. The oxide bound Fe was calculated by subtracting the weakly bound Fe measured by Tamm extraction (Tamm, 1922) from the CBD extracted Fe (Mehra and Jackson, 1960) and the silicate bound Fe was calculated by subtracting the weakly-bound and oxide bound Fe from the total Fe. P0, P50, P300, P700, and P1000 are sites with 0, 50, 300, 700, and 1000 years of rice cultivation history.

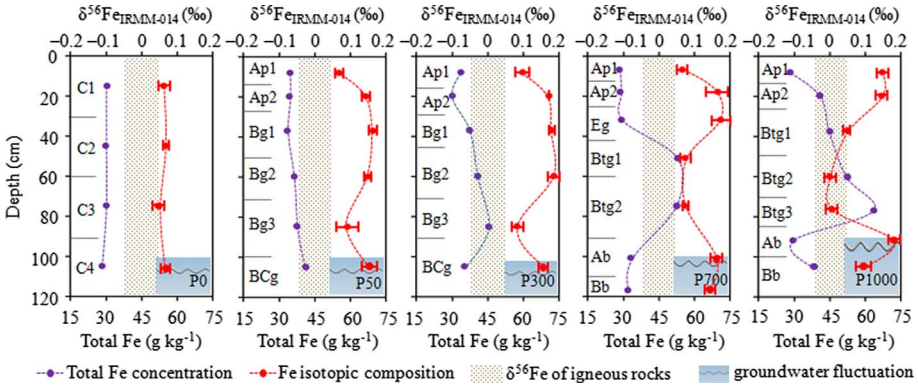

Fig. 3. Distributions and variations of the Fe isotopic compositions (δ^{56}Fe) along the soil depth and chronosequence. Error bars represent 2 SD of replicate measurements. P0, P50, P300, P700, and P1000 are sites with 0, 50, 300, 700, and 1000 years of rice cultivation history.

1985; Zhang and Gong, 1993, 2003; Han and Zhang, 2013). The artificial and seasonal water saturation and drainage during continuous paddy cultivation are expected to cause changes in soil pH and Eh (Kyuma, 2004), which would result in coupled reduction-oxidation and eluviation-illuviation processes of Fe in paddy soils (Gong, 1983; Zhang and Gong, 2003) and thus lead to the formation of diagnostic horizons and features (Fig. 1b, and Table S1 in Supplementary File S1) characterizing Fe distribution and redistribution as paddy soils age. In addition to the artificial submergence and drainage, seasonal fluctuations of groundwater level also induce changes in soil redox potential (Ponnamperuma, 1972; Kirk, 2004) that favor Fe reduction and depletion in the lower horizons of paddy soils (Fig. 2).

Our results demonstrate that both artificial submergence and fluctuation of the groundwater level are involved in the mobilization and translocation of Fe during paddy soil evolution. This results in changes in Fe fluxes and contributions of different Fe pools to total Fe within 0–120 cm soil layer (Fig. 4). Total Fe and oxide bound Fe increased consistently from 47 and 5 kg m^{-2}, respectively, in the uncultivated soil to 69 and 23 kg m^{-2} after 1000 years of rice cultivation (Fig. 4a). The average increasing rate of total Fe (0.32 kg m^{-2} yr^{-1}) and oxide bound Fe (0.19 kg m^{-2} yr^{-1}) during the first 50 years of rice cultivation was, respectively, 36- and 28-fold greater than that between 50- and 1000-yrs time period (Fig. 4a). The silicate bound Fe increased gradually from 31 kg m^{-2} in the uncultivated soil to 46 kg m^{-2} in the 50-yr paddy soil and then remained relatively constant in the progressively older paddy soils (Fig. 4a). The weakly bound Fe decreased at a rate of 0.12 kg m^{-2} yr^{-1} during the initial 50 years of rice cultivation while it showed minimal changes thereafter (Fig. 4a). Silicate bound Fe made up the largest proportion of total Fe across the studied paddy soil chronosequence (Fig. 4b). The contribution of silicate bound Fe and weakly bound Fe to total Fe decreased as paddy soils age, while the proportion of oxide bound Fe to total Fe increased with pedogenic time (Fig. 4b).

The net accumulation of Fe during paddy soil evolution over a millennial time scale, as confirmed by a combination of increasing total Fe concentration (Fig. 2), the positive values of $\tau_{Ti,Fe}$ in most paddy soil horizons (Table S3 in Supplementary File S1) and the elevated total Fe fluxes (Fig. 4a) within 120 cm profile, suggests the external Fe input through artificial flooding and/or atmospheric deposition exceeds the internal Fe loss through the potential Fe leaching. Our results contrast markedly with the observation that rice cultivation over a decadal time scale could significantly enhance Fe depletion in the acid paddy soils developed on sloping upland areas (Zhang and Gong, 2003; Han and Zhang, 2013). Previous studies have shown that the critical redox potentials for Fe reduction and consequent dissolution are between + 300 mV and + 100 mV at pH 6–7, and − 100 mV at pH 8, while at pH 5 appreciable Fe reduction occurred at + 300 mV (Gotoh and Patrick, 1974). The pH value of our paddy soils derived from calcareous parent materials ranged from 6.3 to 8.6 (Table S2 in Supplementary File S1). The alkaline environment at the initial stage (0–50 years) of paddy soil evolution (Table S2 in Supplementary File S1) would impede loss of Fe from the profile, and thus an initial period of Fe accumulation is observed (Fig. 4). As pedogenesis proceeds and $CaCO_3$ is gradually removed from the profile, the soil pH decreases (Table S2 in Supplementary File S1) and Fe accumulates at a lower rate in the later stages of paddy soil evolution (Fig. 4). In comparison, the acid paddy soils with pH values ranging from 4.4 to 6.2 (Zhang and Gong, 2003; Han and Zhang, 2013) have been reported to promote Fe mobilization and leaching loss after artificial flooding irrespective of the similar extrinsic pedogenic environment (external drivers). In addition to the differences in parent materials, paddy soils developed on the sloping upland areas would have a higher leaching potential than those developed on the plain areas. This is confirmed by the rapid decrease of clay content in the sloping upland paddy soils (Zhang and Gong, 2003; Han and Zhang, 2013) as compared with the gradual clay enrichment in our study (Table S2 in Supplementary File S1). Particle-facilitated leaching and transport of nutrients or metals have been extensively reported in the literature (e.g., de Jonge et al., 2004; Mohanty et al., 2014; Lu et al., 2016), which may partly explain the rapid decrease Fe of in acid paddy soils developed on the sloping upland areas. To sum up, the rates and trajectories of Fe evolution in paddy soils are determined by a combination of internal and external factors, including the characteristic of originals soil, paddy soil age, landscape types and positions, and anthropogenic managements.

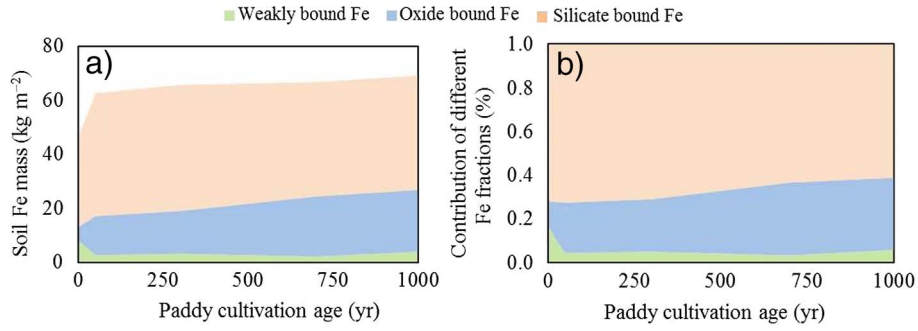

Fig. 4. Changes in Fe fluxes and the contributions of different Fe pools to total Fe within 0–120 cm soil layer during paddy soil development over a millennial time scale. The sum of the area covered by weakly bound Fe, oxide bound Fe and silicate bound Fe (Fig. 5a) represents the total Fe in soils. Note: the assumed linear change in individual Fe pools in this study may not reflect the actual rates over the course of paddy soil development.

4.2. Factors and processes controlling Fe isotope fractionation during paddy soil evolution

The uniform Fe isotopic composition with depth in the uncultivated pedon (P0, Fig. 3) is consistent with that reported by Wiederhold et al. (2007a) and Fekiacova et al. (2013) for Cambisols and suggests no vertical differentiation of Fe isotopic composition occurred prior to the establishment of the paddy soil cultivation. Fe isotopic composition of the paddy soil profile becomes increasingly differentiated with increasing paddy cultivation history (Fig. 3). The $\Delta^{56}Fe_{profile}$ (i.e., the difference between the highest and lowest $\delta^{56}Fe$ values in a given soil profile) of P0, P50, P300, P700, and P1000 is 0.02, 0.09, 0.10, 0.10 and 0.19, respectively, which tends to increase with paddy cultivation age. The significant positive correlation between $\Delta^{56}Fe_{profile}$ and paddy cultivation time ($r = 0.86$, $p < 0.05$) demonstrates that the prolonged paddy cultivation results in larger Fe isotope fractionation. Fe isotope fractionation in soils can be mediated by abiotic processes (proton-promoted or ligand-controlled Fe dissolution and mobilization, Fe adsorption and precipitation, and mineral transformation) as well as biotic processes (microbial reduction or oxidation of Fe) (Fantle and DePaolo, 2004; Emmanuel et al., 2005; Thompson et al., 2007; Wiederhold et al., 2007a, 2007b; Yamaguchi et al., 2007; Buss et al., 2010; Kiczka et al., 2011; Yesavage et al., 2012; Mansfeldt et al., 2012; Fekiacova et al., 2013; Akerman et al., 2014; Schuth et al., 2015; Garnier et al., 2017; Li et al., 2017). In paddy soils, both artificial flooding and variation of the groundwater level are involved in the reduction-oxidation and eluviation-illuviation processes of Fe (Gong, 1983; Zhang and Gong, 2003). This results in a bimodal forcing of Fe translocation and redistribution within the vertical profile in the plant-rooting zone as well as near the permanent groundwater table (Figs. 2 and 3). There is a strong negative correlation between $\delta^{56}Fe$ values and the logarithm of total Fe concentrations in our paddy soils (Fig. S3), indicating the preferential loss of lighter Fe isotopes in the Fe-depleted horizons and enrichments of heavier Fe isotopes in these Fe-depleted zones. This has been confirmed by relatively higher $\delta^{56}Fe$ values in eluvial horizons and lower $\delta^{56}Fe$ values in the illuvial horizons (Fig. 3, Tables S2 and S3 in Supplementary File S1). In addition, the Ab horizons of 700-yr (P700, 90–112 cm) and 1000-yr (P1000, 85–100 cm) paddy profile, which were buried A horizons rich in humus and depleted in Fe, also confirmed the enrichment of heavier Fe isotopes in Fe-depleted horizons (Fig. 3, Tables S2 and S3 in Supplementary File S1). However, given the large variations of Fe concentration (Fig. 2), the mass-dependent Fe isotope fractionation effects in our paddy soils is relatively small compared with other redoximorphic soils (Wiederhold et al., 2007a). This suggests that other pedogenic processes could mask the Fe isotope effects induced by the reduction-oxidation and eluviation-illuviation processes of Fe in paddy soils.

We propose a conceptual model of Fe transfer and redistribution during paddy soil evolution based on changing moisture regimes and redox conditions and interpret their potential impacts on soil Fe isotope compositions (Fig. 5). As an open system, paddy soil receives external inputs of Fe from irrigation and rice straw (Fig. 5), which is expected to result in an enrichment of light Fe isotopes in the surface soil because of the widely reported lighter Fe isotope compositions in rivers (Bergquist and Boyle, 2006; Song et al., 2011; Chen et al., 2014b) and rice straws (Garnier et al., 2017). In contrast, the $\delta^{56}Fe$ values of surface paddy soils were greater than that of uncultivated soil (Fig. 3, and Table S3 in Supplementary File S1). This can be partly attributed to the rice uptake of Fe with lighter Fe isotope as reported by Garnier et al. (2017). On the other hand, the reductive dissolution of Fe-bearing minerals and transfer of Fe under reducing condition will cause an enrichment of heavier and lighter Fe isotopes in the cultivated and illuvial horizon, respectively (Fig. 5). Schuth et al. (2015) have demonstrated that removal of Fe from the topsoil causes progressively higher soil $\delta^{56}Fe$ values due to the preferential release of ^{54}Fe. The vertical movement of low-$\delta^{56}Fe$ solution from the topsoil results with time in the formation of a subsoil with $\delta^{56}Fe$ values that are lower than the topsoil after repeated low and high Eh cycles (Schuth et al., 2015). Similarly, the groundwater fluctuation induced reductive dissolution and transport of Fe will result in an enrichment of heavier and lighter Fe isotopes in the horizon near groundwater level and deeper horizons, respectively (Fig. 5). In addition, the lighter Fe isotopes can be leached out of the pedon causing the enrichment of heavier Fe isotopes in the residual soil (Fig. 5). Therefore, the Fe isotope composition of a specific soil horizon is a result of a complex interaction of different processes. Because the Fe concentrations and isotopic compositions of rice litters, irrigation water, and groundwater in the studied area may vary significantly from those cited in the literature, further investigations of Fe concentrations and isotopic compositions in the soil-plant-water system would better explain the pathways of Fe cycling during paddy soil evolution as illustrated in our proposed model (Fig. 5).

4.3. The stable Fe isotope fingerprints of pedogenetic Fe evolution: a meta-analysis of soil $\delta^{56}Fe$ values in the published literature

Fe isotope variations in bulk soil samples have been reported in many previous studies (e.g., Fantle and DePaolo, 2004; Emmanuel et al., 2005; Thompson et al., 2007; Wiederhold et al., 2007a, 2007b; Yamaguchi et al., 2007; Poitrasson et al., 2008; Kiczka et al., 2011; Mansfeldt et al., 2012; Yesavage et al., 2012; Fekiacova et al., 2013; Akerman et al., 2014; Schuth et al., 2015; Garnier et al., 2017; Li et al., 2017), which provide valuable information for the interpretation of the stable Fe isotopes as a tracer of pedogenetic Fe evolution. A compilation of the Fe isotopic compositions in the bulk soils derived from different parent materials and from different bioclimatic zones are presented in Table 1 and Fig. 6. In contrast to the homogeneous Fe isotopic compositions in the igneous rocks ($\delta^{56}Fe = 0.00 \pm 0.05$‰), bulk soil samples show large variations of $\delta^{56}Fe$ values ranging from −0.61‰ to 1.04‰ (Table 1 and Fig. 6). The heterogeneous Fe isotopic compositions reported in the worldwide soils (Table 1 and Fig. 6) indicate that significant Fe isotope fractionations occur during continental weathering and/or subsequent soil formation, resulting in differentiation of Fe isotopic composition relative to the igneous rocks with trajectories that depend on the controlling environmental conditions (Fig. 6 and Table 1).

Our analysis of global distribution of soil Fe isotopic composition (Table 1 and Fig. 6) demonstrates that Fe isotope fractionation processes occur at various spatial scales (i.e., pedon-, regional and global scales). At the pedon-scale, significant Fe isotope fractionation ($\Delta^{56}Fe_{profile} > 0.15$‰, i.e., the difference between the highest and lowest $\delta^{56}Fe$ values in a given soil profile) has been observed along the vertical soil profile in most of the studied pedons (Table 1 and Fig. 6). The largest in profile Fe isotope variation ($\Delta^{56}Fe_{profile} = 1.16$) occurs in a Ferralsol profile from a semi-arid area in Botswana (Yamaguchi et al., 2007), which is followed by that of Plinthosol ($\Delta^{56}Fe_{profile} = 0.74$), Podzol ($\Delta^{56}Fe_{profile} = 0.11$–$0.76$), Gleysol ($\Delta^{56}Fe_{profile} = 0.07$–$0.41$), Andosol ($\Delta^{56}Fe_{profile} = 0.30$), Albeluvisol ($\Delta^{56}Fe_{profile} = 0.26$) and Anthrosol (i.e., the studied paddy soils) ($\Delta^{56}Fe_{profile} = 0.19$) (Table 1, Table S3 and Fig. 6). Four Cambisol and two Ferralsol profiles developed under oxic and well-drained conditions, however, exhibit little variation of Fe isotopic compositions ($\Delta^{56}Fe_{profile} \leq 0.15$) (Table 1 and Fig. 6). The lack of large Fe isotope fractionation in these soil profiles is attributed to different mechanisms: (i) Poitrasson et al. (2008) suggested that Fe remained mostly in its oxidized form during Ferralsol evolution and thus resulted in little variation of Fe isotopes in the Ferralsol profile; (ii) Wiederhold et al. (2007a) and Fekiacova et al. (2013) concluded that there was limited exchange between different Fe pools and no significant Fe translocation during Cambisol evolution, which impeded the Fe isotope fractionation in the Cambisol profile. Nevertheless, the pedon-scale Fe isotope fractionation occurs in nature when the pedogenic conditions favor the mobilization and vertical translocation of Fe during soil evolution, resulting in the profile

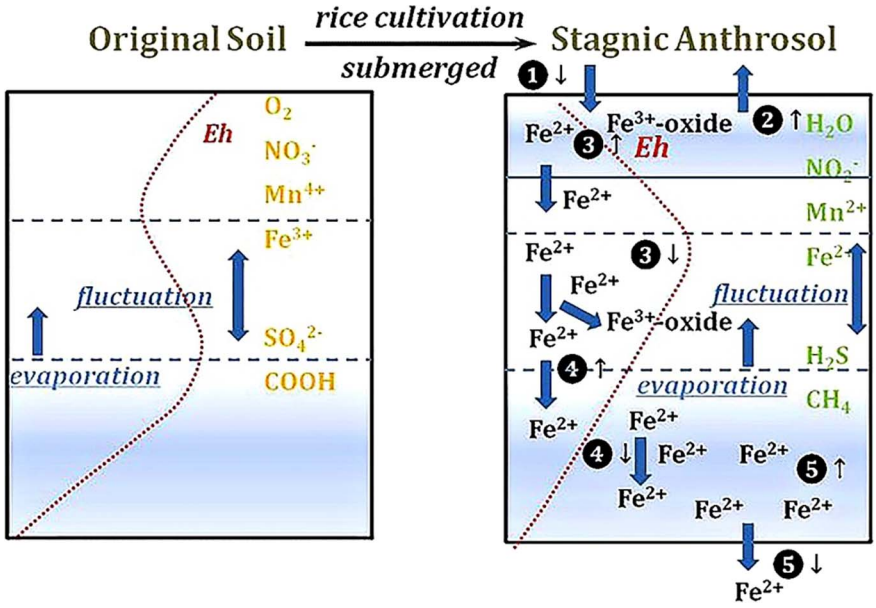

Fig. 5. Conceptual model of Fe transfer and redistribution processes in the studied paddy soil chronosequence and their potential impacts on Fe isotopic compositions in the soil profile with changing moisture regimes and redox conditions. ❶ External input of Fe with lighter Fe isotopes by irrigation and rice straw return (↓); ❷ Rice uptake of Fe with lighter Fe isotopes, leading to the enrichment of heavier Fe isotopes in the cultivated horizon (↑); ❸ Reductive dissolution of Fe-bearing minerals in the cultivated horizon and transfer of lighter Fe isotopes to the illuvial horizons, causing the enrichment of heavier and lighter Fe isotopes in the cultivated (↑) and illuvial horizon (↓), respectively; ❹ Groundwater fluctuation induced reductive dissolution of Fe-bearing minerals and transport of lighter Fe isotopes to the lower horizons, resulting in the enrichment of heavier and lighter Fe isotopes in the horizon near groundwater level (↑) and deeper horizons (↓), respectively; ❺ Lighter Fe isotopes leaching out of pedon, causing the enrichment of heavier Fe isotopes in the residual soil (↑).

differentiation of Fe isotopic compositions as shown in Fig. 6 and Table 1. Furthermore, significant Fe isotope fractionation has also been observed at the regional scale. This is because that the different soil types developed on the same parent material within the similar bioclimatic zones show distinct Fe isotopic compositions and different ranges of δ^{56}Fe values (Thompson et al., 2007; Yesavage et al., 2012; Fekiacova et al., 2013) (Table 1 and Fig. 6). For instance, Thompson et al. (2007) showed different Fe isotopic compositions in an Andosol profile (δ^{56}Fe = 0.15‰–0.45‰) and two Cambisol profiles (δ^{56}Fe = −0.19‰–0.23‰ and δ^{56}Fe = 0.15‰–0.72‰) developed on basalt in Hawaiian Island in a tropical region (Table 1). Yesavage et al. (2012) found that the δ^{56}Fe values of a Cambisol and Plinthosol profile derived from Silurian shale in a temperate region varied from −0.12‰ to 0.29‰ and from −0.03‰ to 0.25‰, respectively (Table 1). Fekiacova et al. (2013) also demonstrated distinct Fe isotope ratios among the Cambisol (δ^{56}Fe = 0.00‰–0.15‰), Albeluvisol (δ^{56}Fe = 0.00‰–0.26‰) and Gleysol (δ^{56}Fe = −0.15‰–0.22‰) profile, all of which are derived from schist in a temperate region (Table 1). It is expected that the mechanisms and pedogenic processes that control the regional soil Fe isotope fractionation differ among various soil types, even though they have the same parent material and evolve under similar environmental conditions. This results in the regional soil diversity, which can partly be expressed by the distinct soil Fe isotopic signatures (Table 1). Finally, the large Fe isotope variations both within soil types—but from different regions—and in the different soil types from different bioclimatic zones (Table 1 and Fig. 6) suggest that Fe isotope fractionating processes could also occur at the global scale, leading to the different degrees of deviation of δ^{56}Fe values in worldwide soils as compared with that of igneous rocks (Fig. 6).

The investigation of Fe isotope variations in soil chronosequences (Kiczka et al., 2011 and this study) (Table 1 and Fig. 6) indicates that the Fe isotope fractionations occur at both short- and long-term pedogenic time scales. At the decadal time scale, our calcareous paddy soil slightly enriches in heavy Fe isotopes in the soil profile (δ^{56}Fe = 0.07‰–0.16‰ in P50 profile) compared with that of parent materials (δ^{56}Fe = 0.05‰–0.07‰ in P0 profile) (Fig. 3). At the centenary to millennial time scale, the enrichment of heavy Fe isotopes in the Fe-depleted horizons and enrichment of light Fe isotopes in the Fe-enriched horizons become more evident as paddy soils age (Fig. 3). In addition, the observed Fe isotope variations in a young (150-yr) glacier chronosequence (Kiczka et al., 2011) (Table 1 and Fig. 6) and in an old Ferralsol profile (up to several millions of years) (Yamaguchi et al., 2007) (Table 1 and Fig. 6) also support the short- and long-term pedogenic Fe isotope fractionations, but the latter amplifies Fe isotopic variations.

The global soil variation in Fe isotopic composition corresponds with large variations of Fe concentration (Fig. 6 and Fig. 7), demonstrating the potential of using stable Fe isotopes as a tool to record pedogenetic Fe evolution. While there is no global relationship between Fe isotopic composition and total soil Fe concentration across different soils (Fig. 7), strong negative correlations between δ^{56}Fe values and the logarithm of total Fe concentrations are frequently observed for certain soil types. For instance, Podzol (r = 0.4994, n = 46, p < 0.001), Gleysol (r = 0.7001, n = 47, p < 0.001), and Stagnic Anthrosol (r = 0.4794, n = 29, p < 0.01) profiles (Fig. 7), all exhibit negative δ^{56}Fe vs. log Fe relationships and these soil types all have Fe mobilization and translocation as key processes during pedogenesis (Emmanuel et al., 2005; Wiederhold et al., 2007a, 2007b; Chen et al., 2011; Mansfeldt et al., 2012; Fekiacova et al., 2013). The previous laboratory work indicates that the reduction- (Beard et al., 1999; Crosby et al., 2005, 2007) and ligand-promoted (Brantley et al., 2001, 2004; Wiederhold et al., 2006) dissolution of Fe minerals preferentially releases light Fe isotopes into solution, resulting the residual solid enriched in heavy Fe isotopes. In natural environments, large Fe isotope fractionations only occur when significant quantities of Fe are separated or mobilized either by redox changes or differences in bonding (Johnson et al., 2008). The Podzols developed under well-drained conditions are characterized by low pH values. Under the acidic conditions, Fe minerals could be dissolved by organic acids and the isotopically light Fe released to the solution could be vertically translocated in the form of Fe^{2+} and/or organic-Fe(II) complexes. Therefore, the bleached and Fe-depleted horizon enriches in isotopically heavy Fe, while light Fe isotopes precipitate in the dark accumulation horizon with abundant illuviated humus and Fe compounds (Emmanuel et al., 2005; Wiederhold et al., 2007a). The Gleysols developed under poorly-drained conditions are subjected to redox oscillations due to changes in water saturation status. The reductive dissolution of Fe would preferentially affect the light isotopes, which could become mobile under reducing conditions. As a result, the residual soil becomes isotopically heavier, while the soil horizons where Fe accumulation occurs become enriched in lighter Fe isotopes (Wiederhold et al., 2007b; Mansfeldt et al., 2012; Fekiacova et al., 2013). The Stagnic Anthrosol formed under the periodic artificial submergence and drainage involves the eluviation-illuviation and oxidation-reduction processes of Fe (Gong,

Table 1
Site description and isotope compositions of total Fe in worldwide soils in published literature.

Location	Climate	MAP[a]	MAT[b]	Vegetation	Parent material	Soil type		N[e]	δ^{56}Fe range	$\Delta^{56}Fe_{profile}$[f]	Reference
		mm	C			WRB[c]	Original[d]		‰		
Mendocino, California, USA	Mediterranean	1270	12	Pine, fir, redwood	Marine sediments	Plinthosol	Phinthic Haplohumults	4	−0.61–0.13	0.74	Fantle and DePaolo (2004)
Shaar Hagay area, Israel	Mediterranean	360	20	Semi-arid vegetation	Limestone/dolomite	Cambisol	Haploxerept	3	−0.21 to −0.13	0.08	Emmanuel et al. (2005)
Načetín, Czech Republic	Temperate	900	5	Forest	Quartzite/gneiss	Podzol	Haplorthods	6	−0.31 to −0.07	0.24	
Hawaiian Island, USA	Tropical	2200	16	Rainforest	Basalt	Cambisol[g]	Andic Dystrudept	2	0.05–0.23	0.18	Thompson et al. (2007)
		2800				Cambisol[g]	Andic Dystrudept	2	−0.19–0.18	0.37	
		3500				Andosol	Acrudoxic Hydrudand	6	0.15–0.45	0.30	
		4200				Gleysol[g]	Aquandic Epiaquept	2	0.39–0.72	0.33	
Flaesheim, Germany	Temperate	822	9	Pine trees	Sand deposit	Podzol	Haplic Podzol	12	−0.29–0.47	0.76	Wiederhold et al. (2007a)
Klosterreichenbach, Germany		689	11	Spruce and pine trees	Sandstone	Podzol	Haplic Podzol	12	−0.02–0.51	0.53	
Immendingen, Germany	Temperate	689	11	Beech trees	Basaltic tuff	Cambisol	Haplic Cambisol	4	0.11–0.21	0.10	
Rafz, Switzerland	Temperate	1086	8.6	Spruce trees	Moraine deposit	Cambisol	Stagnic Cambisol	5	0.01–0.15	0.11	Wiederhold et al. (2007b)
Tettnang, German		828	8.5	Deciduous trees	Sand sediments	Gleysol	Haplic Gleysol	6	0.01–0.27	0.25	
Gaborone, Botswana	Semi-arid	400	21	No data	Basalt	Ferralsol	Oxisol	15	−0.12–1.04	1.16	Yamaguchi et al. (2007)
Nsimi site, Cameroon	Equatorial	1630	24	Rainforest	Granodiorite	Ferralsol	Oxisol	8	0.05–0.15	0.10	Poitrasson et al. (2008)
						Ferralsol	Oxisol	7	0.04–0.18	0.14	
Damma glacier, Switzerland	Glacial	2000	2.2	Grass, shrubs	Granite	Leptosol[h]	Hyperskeletic Leptosol	10	0.10–0.27	0.17	Kiczka et al. (2011)
						Cambisol	Haplic Cambisol	2	0.13–0.14	0.01	
Rhine-Westphalia, Germany	Temperate	783	9.6	Grass	Fluvial deposits	Gleysol	Haplic Gleysol	4	−0.22–0.14	0.36	Mansfeldt et al. (2012)
Susquehanna Shale Hills, Pennsylvania, USA	Temperate	110	8	Deciduous trees	Silurian shale	Cambisol	Lithic Dystrudept	3	0.24–0.29	0.05	Yesavage et al. (2012)
						Cambisol	Lithic Dystrudept	3	0.15–0.25	0.10	
						Gleysol	Typic Dystrudept	6	−0.12–0.19	0.31	
						Gleysol	Aquic Hapludult	7	−0.03–0.25	0.28	
Kervidy-Naizin Catchment, Brittany County, France	Temperate	909	12	Corn and Wheat	Schist	Cambisol	Haplic Cambisol	6	0.00–0.15	0.15	Fekiacova et al. (2013)
						Albeluvisol	Gleyic Albeluvisol	6	0.00–0.26	0.26	
						Gleysol	Orthic Gleysol	7	−0.15–0.26	0.41	
Nsimi site, Cameroon	Equatorial	1630	24	Rainforest	Granodiorite	Gleysol[i]	Histic Gleysol	4	0.33–0.49	0.16	Akerman et al. (2014)
						Gleysol[i]	Histic Gleysol	5	0.40–0.47	0.07	
						Gleysol[i]	Histic Gleysol	2	0.20–0.34	0.14	
						Ferralsol	Ferric Ferralsol	5	0.09–0.15	0.06	
						Ferralsol	Ferric Ferralsol	4	0.02–0.16	0.14	
Lavesum, Germany	Temperate	765	10	Grass	Fluvial deposits	Gleysol	Haplic Gleysol	2	−0.13–0.19	0.32	Schuth et al. (2015)
Araihazar Upazila, Bangladesh	Tropical	1600	18	Rice	Marine sediments	Anthrosol	Hydragric Anthrosol	3	0.06–0.10	0.04	Garnier et al. (2017)
British Columbia, Canada	Temperate	3200	12	Spruce, salal and fir	Beach sand	Cambisol	Haplic Cambisol	2	0.13–0.15	0.02	Fekiacova et al. (2017)
						Podzol	Haplic Podzol	4	0.05–0.16	0.11	
						Podzol	Haplic Podzol	6	−0.02–0.20	0.22	
						Podzol	Haplic Podzol	6	0.00–0.25	0.25	
Surigao, Philippines	Tropical	3000	27	No data	Peridotite	Ferralsol	Oxisol	21	−0.03–0.10	0.13	Li et al. (2017)

[a] Mean annual precipitation.
[b] Mean annual air temperature.
[c] Soil types classified according to World Reference Base for Soil Resources (WRB) (IUSS Working Group WRB, 2006).
[d] Soil types described in the original literature.
[e] Number of data points in each soil profile.
[f] Maximum difference in Fe isotope ratios in each soil profile.
[g] Soil samples in the surface (10–20 cm) and subsurface horizon (50–70 cm).
[h] Surface soils with different ages.
[i] Soil samples in the organo-mineral horizon (0–20 cm) with different depth.

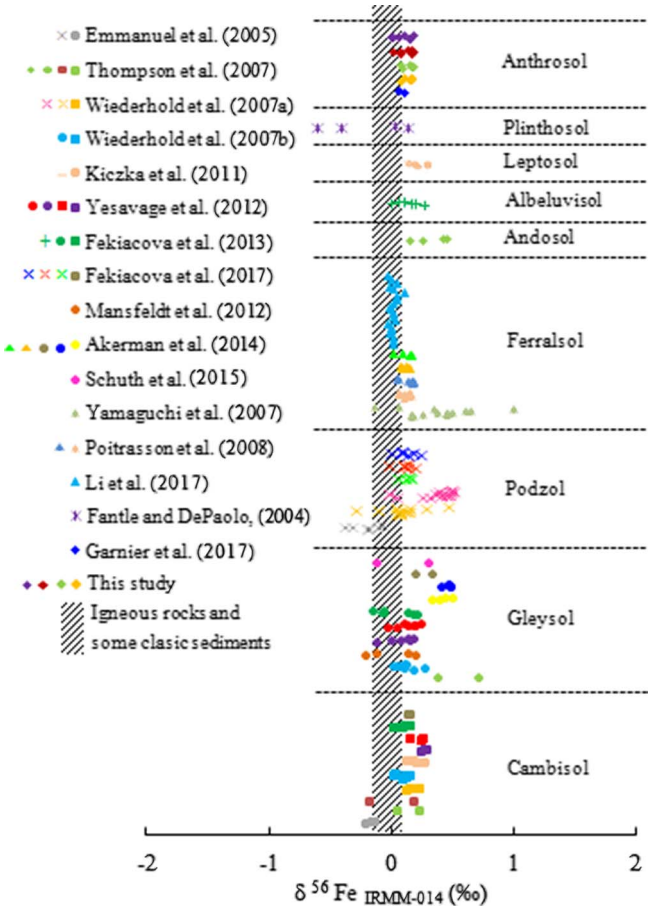

Fig. 6. Summary of Fe isotopic composition of the bulk soils from this study and recent literature. Delta values are expressed relative to IRMM-014 standard, which are average values of repeated measurements. Soil types are translated to WRB (World Reference Base for Soil Resources) (IUSS Working Group WRB, 2006) using the information available. Legends with different colors in each soil type represent δ^{56}Fe value in different soil profiles while the scattered points with the same color represent δ^{56}Fe value in the different horizons in each soil profile. The shaded region between + 0.05‰ and − 0.05‰ represents the range of δ^{56}Fe measured in igneous rocks (Beard et al., 2003). (For interpretation of the references to color in this figure legend, the reader is referred to the web version of this article.)

1983; Chen et al., 2011), resulting in the depletion and accumulation of Fe in the eluvial and illuvial horizon, respectively. The reductive dissolution and translocation of Fe is accompanied by the increase of δ^{56}Fe values in Fe-depleted horizons, leading to the enrichment of light Fe isotopes in the Fe-accumulated horizons (Fig. 3). In addition, the Fe isotopic compositions also record the effects of groundwater on Fe dynamics in the Stagnic Anthrosol by showing slightly heavier Fe isotopes in the horizons near groundwater boundary (Fig. 3). Besides the pedogenic processes discussed above, recent greenhouse and field observations have shown the potential for the aboveground vegetation to influence soil Fe isotopic compositions (Guelke and Von Blanckenburg, 2007; Guelke et al., 2010; Kiczka et al., 2010). The nonlinear (logarithm) relationships between δ^{56}Fe values and total Fe concentrations in Podzol, Gleysol, and Stagnic Anthrosol with different slopes as well as their distinct Fe isotopic signatures (Fig. 7) also suggest that a combination of complex processes control the Fe isotope fractionations, and that the mechanisms responsible for these processes differ among the various soil types. To sum up, Fe isotopes are proven to be a useful tool for studying and distinguishing the various mechanisms and processes that control Fe transfer and evolution in soils, especially when they are used in combination with the pedological and geochemical characterization.

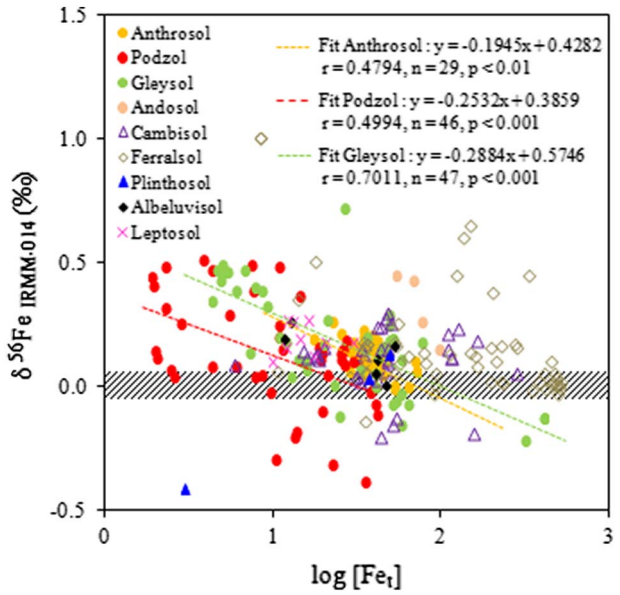

Fig. 7. Relationship between the bulk soil Fe isotopic compositions and total Fe concentrations in the worldwide soils. Data are collected from the published literature and this study. Delta values are expressed relative to IRMM-014 standard, which are average values of repeated measurements.

5. Conclusions

The calcareous paddy soil evolution under the influence of periodic flooding and groundwater fluctuation results in variations of soil moisture regimes and redox conditions with both time and depth that control Fe mobilization, translocation and redistribution, leading to enhanced profile differentiation of Fe oxides and measurable Fe isotope fractionation. The gradual accumulations of profile-scale Fe and Fe oxides in our calcareous paddy soil chronosequence contrasts markedly with the rapid depletion of profile-scale Fe and Fe-oxides in acid paddy soil chronosequences. The rate and trajectory of Fe oxide transformations is influenced by both intrinsic (e.g., characteristics of original soils, paddy soil age) and extrinsic (e.g., landscape types and positions, anthropogenic activities) factors. Mass-dependent Fe isotope fractionation occurs due to the preferential removal of lighter Fe isotopes during long-term paddy soil evolution under the predominant reducing conditions. However, the Fe isotopic ratio of a specific paddy horizon is a result of a complex interaction of different processes, which are summarized and interpreted in our proposed conceptual model. Comparison of Fe isotopic compositions in the worldwide soils demonstrate that Fe isotopes can evidence Fe transfer and pinpoint the factors and processes that control Fe mobilization and redistribution particularly in soils with changing moisture regimes and redox conditions. Our findings provide new insights into the behavior and geochemical cycle of Fe at the Earth's surface strongly affected by human activities and contributes to an improved understanding of anthropedogenesis in the Earth's Critical Zone.

Acknowledgements

We are grateful to Decheng Li, Institute of Soil Science, Chinese Academy of Sciences, and Hong Lu, Cixi Agriculture Bureau, Zhejiang Province, for their help during the field work. We also thank Alan Matthews, Ami Nishri, Jan Wiederhold, Nadya Teutsch, Stephan Kraemer, and Yigal Erel for their patient training on Fe column chemistry and Fe isotope measurements during FIMIN workshop held at The Hebrew University of Jerusalem, Israel. Two anonymous referees are thanked for comments that helped to improve the manuscript. This study was supported by projects from the Natural Science Foundation of

China (Grant nos. 41601221 and 41571130051), Ministry of Science and Technology of the People's Republic of China (Grant no. 2016YFC0501605), State Key Laboratory of Soil and Sustainable Agriculture, Institute of Soil Science, Chinese Academy of Sciences (Grant no. Y20160003), State Key Laboratory of Soil Erosion and Dryland Farming on the Loess Plateau, Institute of Soil and Water Conservation, Chinese Academy of Sciences (No. A314021402-1602), and Key Laboratory of Ecosystem Network Observation and Modeling, Institute of Geographic Sciences and Natural Resources Research, Chinese Academy of Sciences (Grant no. LENOM2016Q0001).

Appendix A. Supplementary data

Supplementary data to this article can be found online at https://doi.org/10.1016/j.chemgeo.2017.11.030.

References

Akerman, A., Poitrasson, F., Oliva, P., Audry, S., Prunier, J., Braun, J.J., 2014. The isotopic fingerprint of Fe cycling in an equatorial soil–plant–water system: the Nsimi watershed, South Cameroon. Chem. Geol. 385, 104–116.
Aniku, J.R.F., Singer, M.J., 1990. Pedogenic iron oxide trends in a marine terrace chronosequence. Soil Sci. Soc. Am. J. 54, 147–152.
Beard, B.L., Johnson, C.M., Cox, L., Sun, H., Nealson, K.H., Aguilar, C., 1999. Iron isotope biosignatures. Science 285 (5435), 1889–1892.
Beard, B.L., Johnson, C.M., Skulan, J.L., Nealson, K.H., Cox, L., Sun, H., 2003. Application of Fe isotopes to tracing the geochemical and biological cycling of Fe. Chem. Geol. 195, 87–117.
Bergquist, B.A., Boyle, E.A., 2006. Iron isotopes in the Amazon River system: weathering and transport signatures. Earth Planet. Sci. Lett. 248 (1), 54–68.
Bernuzzi, G.C.F., Recalcati, S., 2006. A precious metal: iron, an essential nutrient for all cells. Genes Nutr. 1 (1), 25–40.
Brantley, S.L., Liermann, L., Bullen, T.D., 2001. Fractionation of Fe isotopes by soil microbes and organic acids. Geology 29 (6), 535–538.
Brantley, S.L., Liermann, L.J., Guynn, R.L., Anbar, A., Icopini, G.A., Barling, J., 2004. Fe isotopic fractionation during mineral dissolution with and without bacteria. Geochim. Cosmochim. Acta 68 (15), 3189–3204.
Bremner, J.M., 1960. Determination of nitrogen in soil by the Kjeldahl method. J. Agric. Sci. 55 (01), 11–33.
Brimhall, G.H., Dietrich, W.E., 1987. Constitutive mass balance relations between chemical composition, volume, density, porosity, and strain in metasomatic hydrochemical systems: results on weathering and pedogenesis. Geochim. Cosmochim. Acta 51 (3), 567–587.
Buss, H.L., Mathur, R., White, A.F., Brantley, S.L., 2010. Phosphorus and Iron Cycling in Deep Saprolite.
Chadwick, O.A., Brimhall, G.H., Hendricks, D.M., 1990. From a black to a gray box—a mass balance interpretation of pedogenesis. Geomorphology 3 (3), 369–390.
Chen, L.M., Zhang, G.L., 2009. Parent material uniformity and evolution of soil characteristics of paddy soil chronosequence derived from marine sediments. Acta Pedol. Sin. 46, 753–763 (In Chinese).
Chen, L.M., Zhang, G.L., Effland, W.R., 2011. Soil characteristic response times and pedogenic thresholds during the 1000-year evolution of a paddy soil chronosequence. Soil Sci. Soc. Am. J. 75 (5), 1807–1820.
Chen, L.M., Zhang, G.L., Jin, Z.D., 2014a. Rare earth elements of a 1000-year paddy soil chronosequence: implications for sediment provenances, parent material uniformity and pedological changes. Geoderma 230, 274–279.
Chen, J.B., Busigny, V., Gaillardet, J., Louvat, P., Wang, Y.N., 2014b. Iron isotopes in the Seine River (France): natural versus anthropogenic sources. Geochim. Cosmochim. Acta 128, 128–143.
Chen, L.M., Zhang, G.L., Rossiter, D.G., Cao, Z.H., 2015. Magnetic depletion and enhancement in the evolution of paddy and non-paddy soil chronosequences. Eur. J. Soil Sci. 66 (5), 886–897.
Cooperative Research Group on Chinese Soil Taxonomy, 2001. Chinese Soil Taxonomy. Science Press, Beijing (In Chinese).
Cornell, R.M., Schwertmann, U., 2003. The Iron Oxides: Structure, Properties, Reactions, Occurrences, and Uses, 2nd completely revised and extended edition. Wiley-VCH Verlag GmbH & Co., KGaA, Weinheim.
Crosby, H.A., Johnson, C.M., Roden, E.E., Beard, B.L., 2005. Coupled Fe (II)-Fe (III) electron and atom exchange as a mechanism for Fe isotope fractionation during dissimilatory iron oxide reduction. Environ. Sci. Technol. 39 (17), 6698–6704.
Crosby, H.A., Roden, E.E., Johnson, C.M., Beard, B.L., 2007. The mechanisms of iron isotope fractionation produced during dissimilatory Fe (III) reduction by *Shewanella putrefaciens* and *Geobacter sulfurreducens*. Geobiology 5 (2), 169–189.
de Jong, J., Schoemann, V., Tison, J.L., Becquevort, S., Masson, F., Lannuzel, D., Petit, J., Chou, L., Weis, D., Mattielli, N., 2007. Precise measurement of Fe isotopes in marine samples by multi-collector inductively coupled plasma mass spectrometry (MC-ICP-MS). Anal. Chim. Acta 589 (1), 105–119.
de Jonge, L.W., Moldrup, P., Rubæk, G.H., Schelde, K., Djurhuus, J., 2004. Particle leaching and particle-facilitated transport of phosphorus at field scale. Vadose Zone J. 3 (2), 462–470.
Diaz, M.C., Torrent, J., 1989. Mineralogy of iron oxides in two soil chronosequences of central Spain. Catena 16 (3), 291–299.
Duchaufour, P., Souchier, B., 1966. Note sur une méthode d'extraction combinée de l'aluminium et du fer libres dans les sols. Science du sol 1, 17–29.
Dudal, R., 2005. The sixth factor of soil formation. Eurasian Soil Sci. 38, S60.
Emmanuel, S., Erel, Y., Matthews, A., Teutsch, N., 2005. A preliminary mixing model for Fe isotopes in soils. Chem. Geol. 222 (1), 23–34.
Fantle, M.S., DePaolo, D.J., 2004. Iron isotopic fractionation during continental weathering. Earth Planet. Sci. Lett. 228 (3), 547–562.
FAO, 2006. World Reference Base for Soil Resources 2006. World Soil Resour. Rep. 103 FAO, Rome.
Fekiacova, Z., Pichat, S., Cornu, S., Balesdent, J., 2013. Inferences from the vertical distribution of Fe isotopic compositions on pedogenetic processes in soils. Geoderma 209, 110–118.
Fekiacova, Z., Vermeire, M.L., Bechon, L., Cornelis, J.T., Cornu, S., 2017. Can Fe isotope fractionations trace the pedogenetic mechanisms involved in podolization? Geoderma 296, 38–46.
Garnier, J., Garnier, J.M., Vieira, C.L., Akerman, A., Chmeleff, J., Ruiz, R.I., Poitrasson, F., 2017. Iron isotope fingerprints of redox and biogeochemical cycling in the soil-water-rice plant system of a paddy field. Sci. Total Environ. 574, 1622–1632.
Gong, Z.T., 1983. Pedogenesis of paddy soils and its significance in soil classification. Soil Sci. 35, 5–10.
Gong, Z.T., 1986. Origin, evolution and classification of paddy soils in China. Adv. Soil Sci. 5, 174–200.
Gotoh, S., Patrick, W.H., 1974. Transformation of iron in a waterlogged soil as influenced by redox potential and pH. Soil Sci. Soc. Am. J. 38 (1), 66–71.
Guelke, M., Von Blanckenburg, F., 2007. Fractionation of stable iron isotopes in higher plants. Environ. Sci. Technol. 41 (6), 1896–1901.
Guelke, M., von Blanckenburg, F., Schoenberg, R., Staubwasser, M., Stuetzel, H., 2010. Determining the stable Fe isotope signature of plant-available iron in soils. Chem. Geol. 277 (3), 269–280.
Han, G.Z., Zhang, G.L., 2013. Changes in magnetic properties and their pedogenetic implications for paddy soil chronosequences from different parent materials in south China. Eur. J. Soil Sci. 64 (4), 435–444.
Huang, L.M., Zhang, G.L., Thompson, A., Rossiter, D.G., 2013. Pedogenic transformation of phosphorus during paddy soil development on calcareous and acid parent materials. Soil Sci. Soc. Am. J. 77 (6), 2078–2088.
Huang, L.M., Thompson, A., Zhang, G.L., 2014. Long-term paddy cultivation significantly alters topsoil phosphorus transformation and degrades phosphorus sorption capacity. Soil Tillage Res. 142, 32–41.
Huang, L.M., Thompson, A., Zhang, G.L., Chen, L.M., Han, G.Z., Gong, Z.T., 2015. The use of chronosequences in studies of paddy soil evolution: a review. Geoderma 237, 199–210.
Institute of Soil Science, Chinese Academy of Sciences, 1978. Methods for Soil Physical and Chemical Analysis. Shanghai Sci. and Technol. Press, Shanghai (In Chinese).
IUSS Working Group WRB, 2006. World Reference Base for Soil Resources 2006. World Soil Resour. Rep. 103 FAO, Rome.
Jansen, B., Nierop, K.G.J., Verstraten, J.M., 2003. Mobility of Fe(II), Fe(III) and Al in acidic forest soils mediated by dissolved organic matter: influence of solution pH and metal/organic carbon rations. Geoderma 113, 323–340.
Jickells, T.D., An, Z.S., Andersen, K.K., Baker, A.R., Bergametti, G., Brooks, N., Cao, J.J., Boyd, P.W., Duce, B.A., Hunter, K.A., Kawahata, H., Kubilary, N., laRoche, J., Liss, P.S., Mahwowald, N., Prospero, J.M., Ridgwell, A., Tegen, I., Torres, R., 2005. Global iron connections between desert dust, ocean biogeochemistry, and climate. Science 308 (5718), 67–71.
Johnson, C.M., Skulan, J.L., Beard, B.L., Sun, H., Nealson, K.H., Braterman, P.S., 2002. Isotopic fractionation between Fe (III) and Fe (II) in aqueous solutions. Earth Planet. Sci. Lett. 195 (1), 141–153.
Johnson, C.M., Beard, B.L., Roden, E.E., 2008. The iron isotope fingerprints of redox and biogeochemical cycling in modern and ancient earth. Annu. Rev. Earth Planet. Sci. 36, 457–493.
Kaiser, K., Guggenberger, G., 2000. The role of DOM sorption to mineral surfaces in the preservation of organic matter in soils. Org. Geochem. 31, 711–725.
Kiczka, M., Wiederhold, J.G., Kraemer, S.M., Bourdon, B., Kretzschmar, R., 2010. Iron isotope fractionation during Fe uptake and translocation in alpine plants. Environ. Sci. Technol. 44 (16), 6144–6150.
Kiczka, M., Wiederhold, J.G., Frommer, J., Voegelin, A., Kraemer, S.M., Bourdon, B., Kretzschmar, R., 2011. Iron speciation and isotope fractionation during silicate weathering and soil formation in an alpine glacier forefield chronosequence. Geochim. Cosmochim. Acta 75 (19), 5559–5573.
Kirk, G., 2004. The Biogeochemistry of Submerged Soils. John Wiley & Sons, Chichester, UK.
Kyuma, K., 2004. Paddy Soil Science. Kyoto University Press, Kyoto, Japan.
Lalonde, K., Mucci, A., Ouellet, A., Ge'linas, Y., 2012. Preservation of organic matter in sediments promoted by iron. Nature 483, 198–200.
Li, M., He, Y.S., Kang, J.T., Yang, X.Y., He, Z.W., Yu, H.M., Huang, F., 2017. Why was iron lost without significant isotope fractionation during the lateritic process in tropical environments? Geoderma 290, 1–9.
Lovley, D.R., Holmes, D.E., Nevin, K.P., 2004. Dissimilatory Fe(III) and Mn(IV) reduction. Adv. Microb. Physiol. 49, 219–286.
Lu, C., Wu, Y., Hu, S., 2016. Drying–wetting cycles facilitated mobilization and transport of metal-rich colloidal particles from exposed mine tailing into soil in a gold mining region along the Silk Road. Environ. Earth Sci. 75 (12), 1–12.
Mansfeldt, T., Schuth, S., Häusler, W., Wagner, F.E., Kaufhold, S., Overesch, M., 2012. Iron oxide mineralogy and stable iron isotope composition in a Gleysol with petrogleyic properties. J. Soils Sediments 12 (1), 97–114.

McFadden, L.D., Hendricks, D.M., 1985. Changes in the content and composition of pedogenic iron oxyhydroxides in a chronosequence of soils in southern California. Quat. Res. 23 (2), 189–204.
Mehra, O.P., Jackson, M.L., 1960. Iron oxide removal from soils and clays by a dithionite-citrate system buffered with sodium bicarbonate. Clay Clay Miner. 7, 317–327.
Mohanty, S.K., Saiers, J.E., Ryan, J.N., 2014. Colloid-facilitated mobilization of metals by freeze–thaw cycles. Environ. Sci. Technol. 48 (2), 977–984.
Nelson, D.W., Sommers, L.E., 1982. Total carbon, organic carbon and organic matter. In: Page, A.L. (Ed.), Methods of Soil Analysis. Part 2, 2nd ed. Agron. Monogr. Vol. 9. ASA and SSSA, Madison, WI, pp. 539–577.
Poitrasson, F., Viers, J., Martin, F., Braun, J.J., 2008. Limited iron isotope variations in recent lateritic soils from Nsimi, Cameroon: implications for the global Fe geochemical cycle. Chem. Geol. 253 (1), 54–63.
Ponnamperuma, F.N., 1972. The chemistry of submerged soils. Adv. Agron. 24, 29–96.
Rudnick, R.L., Gao, G., 2004. Composition of the continental crust. In: Rudnick, R.L. (Ed.), Treatise on Geochemistry: The Crust. Vol. 3. Elsevier, Amsterdam, The Netherlands, pp. 1–64.
Schoenberg, R., von Blanckenburg, F., 2005. An assessment of the accuracy of stable Fe isotope ratio measurements on samples with organic and inorganic matrices by high-resolution multicollector ICP-MS. Int. J. Mass Spectrom. 242 (2), 257–272.
Schoeneberger, P.J., Wysocki, D.A., Benham, E.C., Broderson, W.D., 2002. Field Book for Describing and Sampling Soils, 2nd ed. Natl. Soil Surv. Ctr., Lincoln, NE.
Schuth, S., Hurraß, J., Münker, C., Mansfeldt, T., 2015. Redox-dependent fractionation of iron isotopes in suspensions of a groundwater-influenced soil. Chem. Geol. 392, 74–86.
Song, L., Liu, C.Q., Wang, Z.L., Zhu, X.K., Teng, Y.G., Wang, J.S., Tang, S.H., Liang, L.L., 2011. Iron isotope compositions of natural river and lake samples in the Karst area, Guizhou Province, Southwest China. Acta Geol. Sin. 85 (3), 712–722.
Stucki, J.W., Goodman, B.A., Schwertmann, 1988. Iron in Soils and Clay Minerals. D. Reidel. Springer, Dordrecht, the Netherlands.
Tamm, O., 1922. Eine method zur bestimmung der anorganishen komponenten des golkomplex im boden. Medd. Statens Skogforsoksanst 19, 385–404.
Thompson, A., Ruiz, J., Chadwick, O.A., Titus, M., Chorover, J., 2007. Rayleigh fractionation of iron isotopes during pedogenesis along a climate sequence of Hawaiian basalt. Chem. Geol. 238 (1), 72–83.
Torrent, J., Schwertmann, U., Schulze, D.G., 1980. Iron oxide mineralogy of some soils of two river terrace sequences in Spain. Geoderma 23 (3), 191–208.
van Breemen, N., Buurman, P., 2004. Soil Formation, 2nd ed. Kluwer Acad. Publ., Dordrecht, the Netherlands.
Vodyanitskii, Y.N., 2010. Iron hydroxides in soils: a review of publications. Eurasian Soil Sci. 43 (11), 1244–1254.
Wang, Q.Y., 2004. Evolution History of Seawall in Cixi County, Zhejiang Province. Fang Zhi Press, Beijing (in Chinese).
Wiederhold, J.G., Kraemer, S.M., Teutsch, N., Borer, P.M., Halliday, A.N., Kretzschmar, R., 2006. Iron isotope fractionation during proton-promoted, ligand-controlled, and reductive dissolution of goethite. Environ. Sci. Technol. 40 (12), 3787–3793.
Wiederhold, J.G., Teutsch, N., Kraemer, S.M., Halliday, A.N., Kretzschmar, R., 2007a. Iron isotope fractionation during pedogenesis in redoximorphic soils. Soil Sci. Soc. Am. J. 71 (6), 1840–1850.
Wiederhold, J.G., Teutsch, N., Kraemer, S.M., Halliday, A.N., Kretzschmar, R., 2007b. Iron isotope fractionation in oxic soils by mineral weathering and podzolization. Geochim. Cosmochim. Acta 71 (23), 5821–5833.
Yamaguchi, K.E., Johnson, C.M., Beard, B.L., Beukes, N.J., Gutzmer, J., Ohmoto, H., 2007. Isotopic evidence for iron mobilization during Paleoproterozoic lateritization of the Hekpoort paleosol profile from Gaborone, Botswana. Earth Planet. Sci. Lett. 256 (3), 577–587.
Yesavage, T., Fantle, M.S., Vervoort, J., Mathur, R., Jin, L., Liermann, L.J., Brantley, S.L., 2012. Fe cycling in the Shale Hills Critical Zone Observatory, Pennsylvania: an analysis of biogeochemical weathering and Fe isotope fractionation. Geochim. Cosmochim. Acta 99, 18–38.
Yu, T.R., 1985. Physical Chemistry of Paddy Soils. Science Press, Beijing, China.
Zhang, G.L., Gong, Z.T., 1993. Geochemical features of element migration under artificial submergence. Acta Pedol. Sin. 30, 355–365 (In Chinese).
Zhang, G.L., Gong, Z.T., 2003. Pedogenic evolution of paddy soils in different soil landscapes. Geoderma 115, 15–29.